Geoscience Frontiers 10 (2019) 885–894

HOSTED BY

Contents lists available at ScienceDirect

China University of Geosciences (Beijing)

Geoscience Frontiers

journal homepage: www.elsevier.com/locate/gsf

Research Paper

Zircon U–Pb–Hf constraints from Gongga Shan granites on young crustal melting in eastern Tibet

Nick M.W. Roberts [a,*], Michael P. Searle [b]

[a] NERC Isotope Geosciences Laboratory, British Geological Survey, Environment Science Centre, Nottingham, NG12 5GG, UK
[b] Department of Earth Sciences, University of Oxford, South Parks Road, Oxford, OX1 3AN, UK

ARTICLE INFO

Article history:
Received 28 June 2017
Received in revised form
21 February 2018
Accepted 27 February 2018
Available online 21 March 2018

Keywords:
Tibet
Himalaya
Hf isotopes
Zircon
Crustal melting

ABSTRACT

The Gongga Shan batholith is a complex granitoid batholith on the eastern margin of the Tibetan Plateau with a long history of magmatism spanning from the Triassic to the Pliocene. Late Miocene–Pliocene units are the youngest exposed crustal melts within the entire Asian plate of the Tibetan Plateau. Here, we present in-situ zircon Hf isotope constraints on their magmatic source, to aid the understanding of how these young melts were formed and how they were exhumed to the surface. Hf isotope signatures of Eocene to Pliocene zircon rims ($\varepsilon_{Hf}(t) = -4$ to $+4$), interpreted to have grown during localised crustal melting, are indicative of melting of a Neoproterozoic source region, equivalent to the nearby exposed Kangding Complex. Therefore, we suggest that Neoproterozoic crust underlies this region of the Songpan–Ganze terrane, and sourced the intrusive granites that form the Gongga Shan batholith. Localised young melting of Neoproterozoic lower or middle crust requires localised melt-fertile lithologies. We suggest that such melts may be equivalent to seismic and magnetotelluric low-velocity and high-conductivity zones or "bright spots" imaged across much of the Tibetan Plateau. The lack of widespread exposed melts this age is due either to the lack of melt-fertile rocks in the middle crust, the very low erosion level of the Tibetan plateau, or to a lack of mechanism for exhuming such melts. For Gongga Shan, where some melting is younger than nearby thermochronological ages of low temperature cooling, the exact process and timing of exhumation remains enigmatic, but their location away from the Xianshuihe fault precludes the fault acting as a conduit for the young melts. We suggest that underthrusting of dry granulites of the lower Indian crust (Archaean shield) this far northeast is a plausible mechanism to explain the uplift and exhumation of the eastern Tibetan Plateau.

1. Introduction

The Himalaya–Tibetan orogen, formed through the collision of India and Asia since ~60–50 Ma (Green et al., 2008; Najman et al., 2010, 2017; Decelles et al., 2014; Hu et al., 2016), is the world's largest active orogeny, and has greatly contributed to our knowledge of continental collision processes and mountain belt evolution. Continental collision can lead to regional mid- to lower crust metamorphism and crustal melting, and this in turn forms a key part of orogenic evolution, particularly through melt weakening (e.g. Hollister and Crawford, 1986; Rosenberg and Handy, 2005; Jamieson et al., 2011). Orogenic melting in the Himalaya–Tibetan orogen is most exemplified by the leucogranite bodies (Greater Himalaya leucogranites) that stretch the length of the main orogenic belt, forming many of the largest mountain peaks. These Oligocene–Miocene leucogranites are a key aspect of the Himalayan channel flow model (e.g. Hodges, 2000; Searle et al., 2006, 2010; Streule et al., 2010). This model postulates that melt formation in the middle crust in combination with high erosion rates and gravitational instability, enables the exhumation of a channel of melt-weakened middle crust southward towards the Indian foreland (Nelson et al., 1996; Beaumont et al., 2001; Grujic et al., 2002).

Elsewhere in the Himalaya–Tibetan orogen, orogenic or post-collisional magmatism is more scattered and can be grouped into four domains: (1) a belt of crustal melts exposed within gneiss domes exposed north of the High Himalaya leucogranites and south of the Indus-Yarlung suture zone (Chen et al., 1990; King et al., 2011; Zeng et al., 2011; Hou et al., 2012); (2) adakitic, potassic and ultrapotassic intrusions and volcanics occurring diachronously

* Corresponding author.
E-mail addresses: nirob@bgs.ac.uk, nickmwroberts@gmail.com (N.M.W. Roberts).
Peer-review under responsibility of China University of Geosciences (Beijing).

https://doi.org/10.1016/j.gsf.2018.02.010

across different regions of the Tibetan plateau, and associated with mantle involvement (Miller et al., 1999; Williams et al., 2004; Chung et al., 2005; Guo et al., 2006); (3) localised crustal melts exposed across limited parts of the Tibetan plateau (e.g. Roger et al., 1995; Kapp et al., 2005; Laskowski et al., 2017; Searle et al., 2016; Weller et al., 2016); and (4) "bright spots" imaged in the current middle crust that may represent melting today (Brown et al., 1996; Chen et al., 1996; Makovsky et al., 1996; Wei et al., 2001; Li et al., 2003). The spatial, temporal and geochemically distinct suites of magmatism across the Himalaya–Tibetan orogen provide insight into crustal differentiation and deformation processes during continent collision. This paper examines an example of a localised region of crustal melting near the eastern margin of the Tibetan plateau, known as the Gongga Shan massif. Here we revisit two samples already dated in Searle et al. (2016), presenting new in-situ Hf isotope data from the youngest melts exposed in this long-lived intrusive complex, and we discuss the source and processes behind this very young (Miocene–Pliocene) magmatism.

2. Geological setting

Gongga Shan (7556 m) is the highest mountain in the eastern Tibetan Plateau, and is approximately 2.5 km higher than the average elevation of the plateau (Fig. 1). The Gongga Shan massif is mainly composed of a granitoid complex intruded into the Palaeozoic–Triassic sediments of the Songpan–Ganze terrane (SGT) (Fig. 1). The Songpan–Ganze terrane is comprised of a thick sequence of dominantly Triassic flysch-type sediments that were deposited in a branch of Paleotethys, a basin that was inverted during collision between the Qiangtang, and North and South China Blocks (Roger et al., 2010 and references within). The sediments are highly deformed and dominantly folded into tight upright folds (Harrowfield and Wilson, 2005). Deposition occurred from the Late Permian through to the Upper Jurassic, but is mostly Middle–Upper Triassic (e.g. Chen et al., 1995; Bruguier et al., 1997; Weislogel et al., 2010). Provenance has been addressed in several studies, and is from Kunlun and Qinling–Dabie orogens to the north and east, as well as the South China Block and Yidun arc to the east and south (Weislogel et al., 2006, 2010; Enkelmann et al., 2007; Gehrels et al., 2011; Ding et al., 2013; Zhang et al., 2014, 2015). In the east of the SGT, where Gongga Shan is located, the SGT is bound by exposed Neoproterozoic rocks of the Yangtze craton, specifically the ca. 800 Ma Kangding Complex (Zhou et al., 2002; Chen et al., 2005; Zhao et al., 2008a, b). In places the Gongga Shan intrusives are directly in contact with the Kangding Complex, but this boundary forms a strand of the large regional, dominantly strike-slip, left-lateral Xianshuihe fault (Fig. 1c).

The N–S trending Gongga Shan batholith is over 100 km long but up to only 20 km wide. The outcrop pattern shows how the batholith is clearly cut and offset by strands of the Xianshuihe fault (Fig. 1). These strands shape the Gongga Shan batholith into a left-lateral strike-slip duplex. Field relations show that both ductile

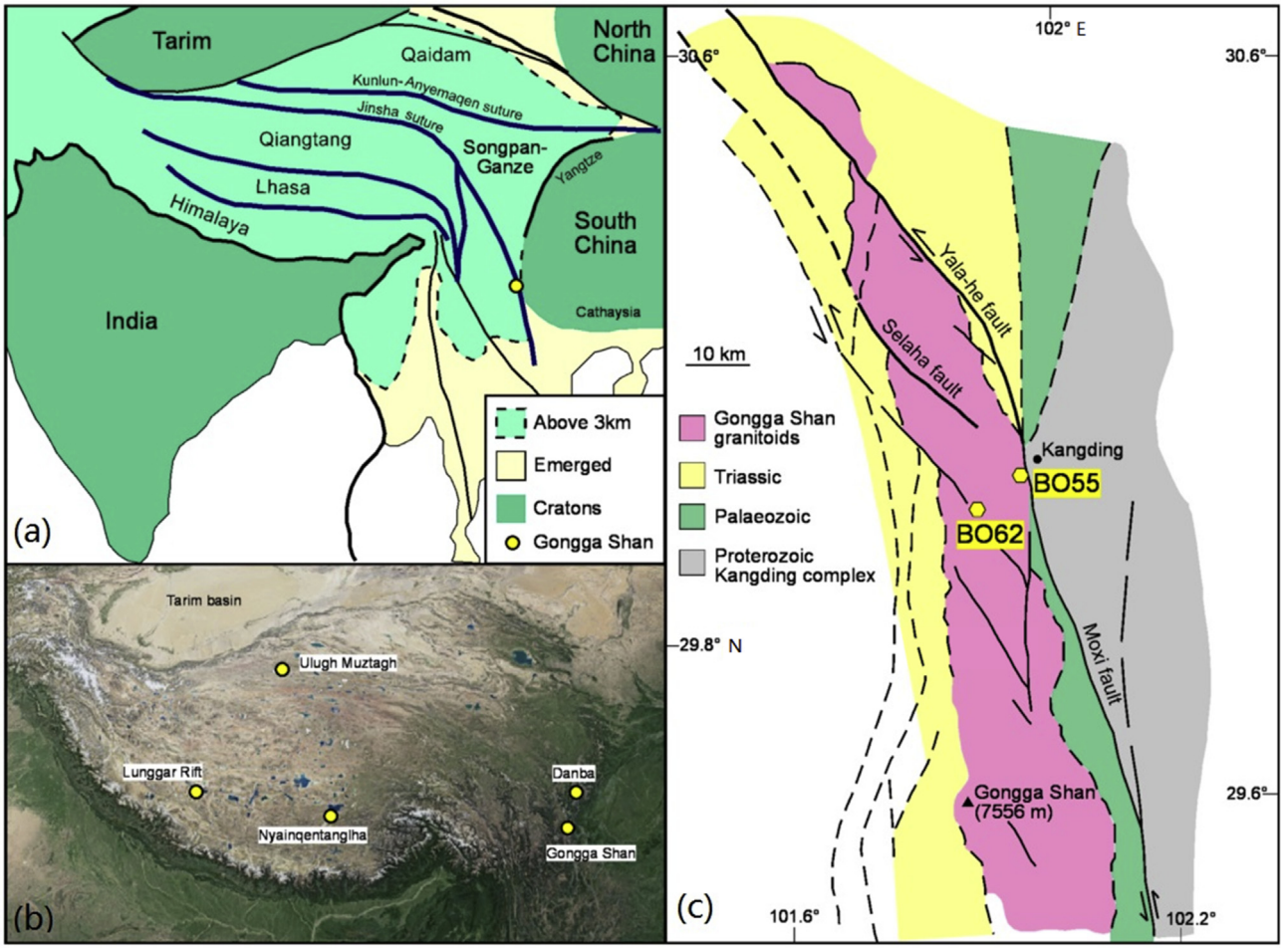

Figure 1. (a) Sketch map of central Asia showing terranes involved in the Himalaya–Tibetan orogeny. (b) Satellite image (Google Earth™) of the Tibetan Plateau showing locations referred to in the text. (c) Simplified geological map of the Gongga Shan batholith and major structures of the Xianshuihe fault, after Searle et al. (2016).

and brittle fault exposures cut Gongga Shan granitoids, indicating they both are younger than the magmatism (Searle et al., 2016). Petrologically, the Gongga Shan batholith comprises a wide range of magma types, with both I- and S-type mineral assemblages (Searle et al., 2016). The I-types include biotite and biotite + hornblende monzogranite, granodiorite and granite. The S-types include biotite + tourmaline granite and pegmatite, garnet + muscovite granite, and biotite + muscovite granite. Some outcrops feature evidence of migmatisation of metasedimentary country rocks, with formation of leucogranites. Other outcrops feature enclaves of more mafic magmatic material, which suggest a role of magma mingling in formation of the granitoid suite (Searle et al., 2016).

Ages for Gongga Shan magmatism can be loosely grouped into four time periods. The earliest group ranges from ca. 216 Ma to 203 Ma, and the second group ranges from ca. 182 Ma to 159 Ma (Li et al., 2015; Searle et al., 2016). Some inheritance of the first group is found in the second group. Allanite ages in four 'group one' granitoids at ca. 174–164 Ma indicate thermal reworking of these earlier granitoids during the second period of magmatism, but titanite and allanite ages of ca. 205 Ma in other 'group one' granitoids suggest that the ca. 182–159 Ma tectono-thermal activity was not pervasive. The third group of granitoids is poorly constrained. It comprises: (1) a pegmatite with populations of zircon ages at 41 Ma (Searle et al., 2016); (2) a migmatitic granite with two zircon ages at ca. 35 Ma (Searle et al., 2016); and (3) a migmatite with zircon populations in the leucosome and melanosome at ca. 32 and 27 Ma respectively (Li and Zhang, 2013). The fourth group ranges from 18 Ma to 4 Ma (Roger et al., 1995; Liu et al., 2006; Li and Zhang, 2013; Li et al., 2015; Searle et al., 2016; Zhang et al., 2017), and also includes allanite ages of 16–5 Ma (Searle et al., 2016).

The tectonic setting during each of the magmatic periods forming the Gongga Shan batholith is poorly constrained. To our knowledge there is no published geochemical study that may help in this regard. Roger et al. (1995) provided some limited whole-rock geochemistry and Pb–Pb, Rb–Sr and Sm–Nd isotopic data, but only one of their samples received combined U–Pb and isotopic analysis, which is requisite in such a complex granitoid complex. Their data provide Nd model ages ranging from 1.49 Ga to 1.24 Ga. Searle et al. (2016) suggested an Andean-type setting during the 215–159 Ma periods of magmatism, although they did not provide specific lines of evidence for this interpretation. This setting would fit the range of I- and S-type lithologies and the protracted nature of the magmatic episodes. The young periods of magmatism are inferred to be related to crustal melting (Roger et al., 1995; Searle et al., 2016), and overlap with on-going convergence in the Himalaya–Tibetan orogen. Li and Zhang (2013) postulated that migmatisation may be related to activity along the Xianshuihe fault zone, but field observations along the Gongga Shan batholith show that the strike-slip faults cut relatively undeformed granite, indicating that faulting post-dated the adjacent granites (Searle et al., 2016).

3. Samples

3.1. BO55

BO55 is an undeformed pegmatitic granite from Shuguang Bridge that cuts across both an earlier biotite monzogranite, which has a weak foliation, and a more leucocratic biotite-muscovite granite that exhibits partial melt structures (schlieren of melanosomes). The migmatitic granite itself intrudes the monzogranite. U–Pb geochronology yielded four old analyses at 159 ± 4 Ma, populations at 41 Ma and 37 Ma and younger dates spreading from 22 Ma to 15 Ma, possibly representing lead-loss, to 15 Ma or even younger (Searle et al., 2016). Allanite yielded two populations of U–Pb age data, one at ca. 173 Ma and one at ca. 15 Ma. The overlap between the allanite age and the youngest zircon led Searle et al. (2016) to suggest the intrusion age was 15 Ma.

3.2. BO62

BO62 is a biotite monzogranite from the middle part of the batholith that is cut by later, minor intrusions of biotite-tourmaline pegmatites and muscovite-garnet granite veins. U–Pb age data (Searle et al., 2016) yielded a strong mixing line between ca. 800 Ma and a Neogene lower intercept. The younger analyses reveal concordant populations at both ca. 14 Ma, and ca. 6–5 Ma. An imprecise allanite lower intercept age of 5 Ma was also determined. Searle et al. (2016) interpreted the data to represent crystallisation of melt at ca. 5 Ma.

4. Method

Lu–Hf isotopes were measured at the NERC Isotope Geosciences Laboratory (Nottingham, UK) using a Thermo Scientific Neptune Plus multi-collector inductively coupled mass spectrometer (ICP-MS) coupled to a New Wave Research 193UC excimer laser ablation system fitted with a TV2 cell. He carrier gas was added to Ar sourced from Cetac Aridus II desolvating nebuliser at a Y-piece before entering the torch. Ablation conditions were 30 μm spots at 10 Hz and a fluence of 6.5 J/cm^2, measured for 30 s. The spots were placed directly over pits previously analysed for U–Pb (presented in Searle et al., 2016). Masses measured are ^{172}Yb, ^{173}Yb, ^{175}Lu, ^{176}Hf + Yb + Lu, ^{177}Hf, ^{178}Hf, ^{179}Hf and ^{180}Hf. A standard–sample–standard bracketing technique using reference zircon 91500 (Wiedenbeck et al., 1995, 2004) was used to correct ^{176}Lu/^{177}Hf and ^{176}Hf/^{177}Hf ratios. Plešovice (Sláma et al., 2008) and the synthetic zircon MUNZirc (Fisher et al., 2011) were used to monitor accuracy and precision of internally corrected Lu and Hf isotope ratios. The reference solution JMC475 was analysed at the start of each analytical session as both undoped and doped with 50 ppb Yb. The correction for ^{176}Yb on the ^{176}Hf peak was made using reverse-mass-bias correction of the ^{176}Yb/^{173}Yb ratio (0.7941), after empirical derivation using the Hf mass bias corrected Yb-doped JMC475 solution measurements (Nowell and Parrish, 2001). The ^{176}Lu interference on the ^{176}Hf peak was corrected using the measured ^{175}Lu and natural ^{176}Lu/^{175}Lu ratio (0.02653) and assuming a mass bias equivalent to Hf. The reproducibility of the ^{176}Lu/^{177}Hf and ^{176}Hf/^{177}Hf measurements of zircon 91500 was approximately 0.45 and 0.01% (2s) respectively. The secondary reference material Plešovice gave a weighted mean ^{176}Hf/^{177}Hf ratio of 0.282468 ± 0.000024 (0.282482 ± 0.000013; Sláma et al., 2008), and MUNZirc gave 0.282156 ± 0.000026 (0.282135; Fisher et al., 2011). Calculation of age-corrected initial ^{176}Hf/^{177}Hf ratios used the decay constant of Söderlund et al. (2004), the CHUR value of Bouvier et al. (2008), and are reported as $\varepsilon_{Hf}(t)$. Data were screened using the ablation signal profiles so that ablations with mixed age domains were excluded.

5. Results

5.1. BO55

Nine analyses were made across nine grains (Fig. 2; Table 1), with the analyses spread across all age domains in the sample. The four Miocene age domains have $\varepsilon_{Hf}(t)$ values ranging from −4.12 to −2.02 (Fig. 3). The three ca. 40 Ma age domains have $\varepsilon_{Hf}(t)$ values of −1.92 to +1.60, and the two Triassic inherited cores have $\varepsilon_{Hf}(t)$ of −2.01 and −0.71. Fig. 3 shows $\varepsilon_{Hf}(t)$ plotted versus apparent (^{206}Pb/^{238}U)

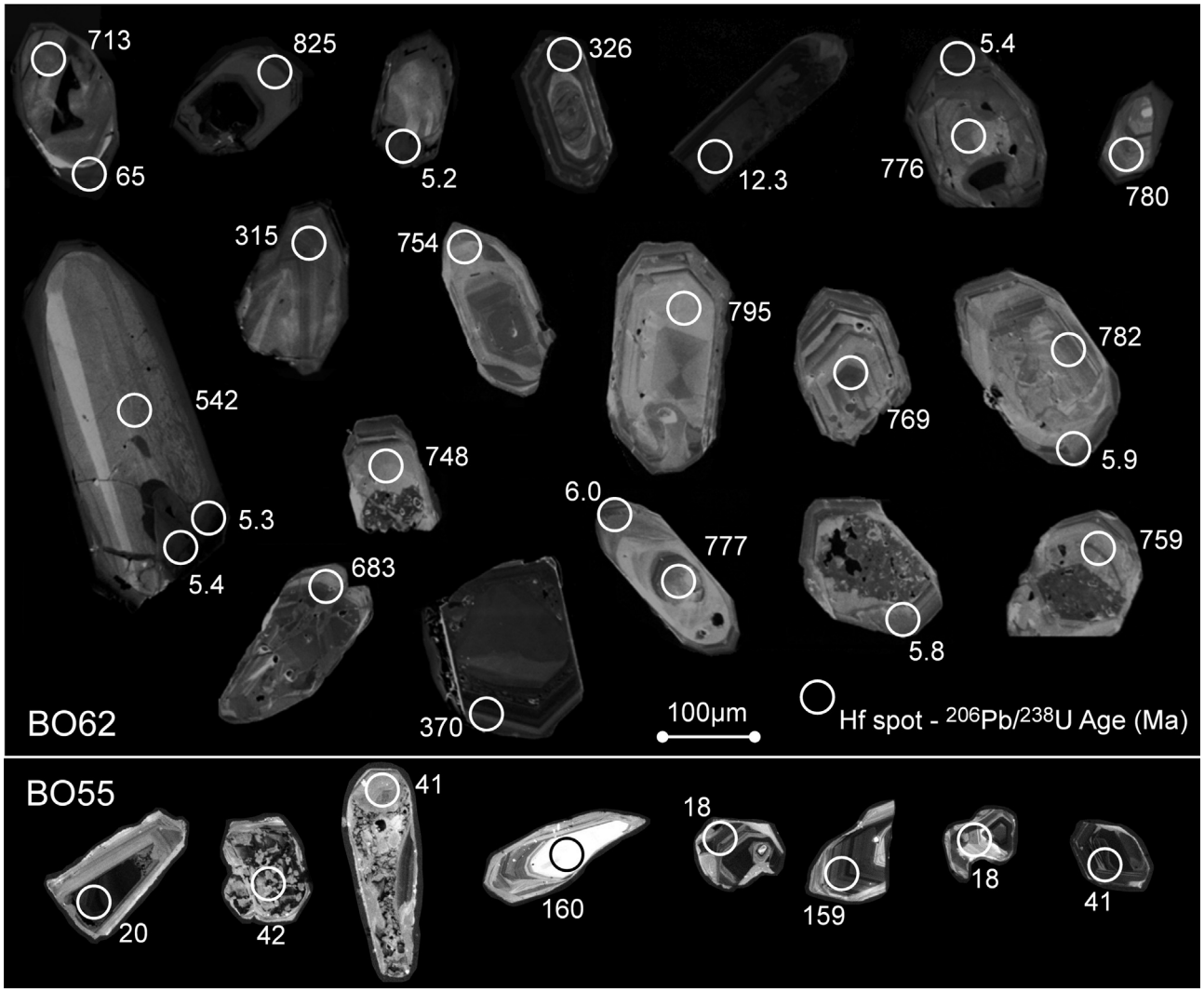

Figure 2. Cathodoluminescence images of selected zircons from samples BO55 and BO62, showing location of spots for Hf isotope analysis and their corresponding age.

age. Lu–Hf evolution trends for zircon lead-loss (Lu–Hf = 0) and the evolution of an average crustal composition (Lu/Hf = 0.015; Griffin et al., 2002) are shown for comparison.

5.2. BO62

Twenty-six analyses were made across nineteen grains (Fig. 2 and Table 1). Of these, eleven correlate with ca. 800 Ma inherited cores, eight correlate with ca. 5 Ma rims, one correlates with a ca. 14 Ma rim, and the other five represent mixtures between these (Fig. 3). The $\varepsilon_{Hf}(t)$ values (Fig. 3) of the 5 Ma rims range from −1.90 to +3.64, and the $\varepsilon_{Hf}(t)$ values of the 800 Ma cores range from +5.16 to +10.10. The analyses that represent age mixtures, probably due to the spots overlapping different age domains, feature $\varepsilon_{Hf}(t)$ signatures that are compatible with physical mixing between the ca. 800 Ma core and ca. 5 Ma rim ages.

6. Discussion

6.1. Magma source

The $\varepsilon_{Hf}(t)$ values of the ca. 14–5 Ma rims on BO62 do not fall on a lead-loss trajectory (i.e. Lu–Hf = 0) from the ca. 800 Ma core $\varepsilon_{Hf}(t)$ values (Fig. 3). This confirms the conclusion of Searle et al. (2016) that the rims represent new zircon crystallisation and/or dissolution-re-precipitation in the presence of melt. The fact that these rim $\varepsilon_{Hf}(t)$ signatures fall on a trajectory representing the evolution of average upper continental crust (i.e. Lu–Hf = 0.015), is compatible with reworking of the 800 Ma source rock without addition of material significantly more juvenile, such as depleted mantle. The signatures of BO55 overlap those of BO62, suggesting a similar magmatic source; this is apparent for both the ca. 41 Ma and ca. 17 Ma rim domains. The $\varepsilon_{Hf}(t)$ signature of the two Triassic zircon domains overlaps the broad evolution of the potential ca. 800 Ma source, suggesting that the inherited magmatic rock in BO55 may also be derived from this Neoproterozoic source.

The $\varepsilon_{Hf}(t)$ signature of potential source rocks is shown in Fig. 3b. The Neoproterozoic cores in BO62 overlap directly with values from the similarly aged Kangding Complex that is exposed to the east of the Gongga Shan batholith (Fig. 1). This provides strong evidence that BO62 is derived from remelting of Kangding Complex crust, or a source region that also produced this Neoproterozoic magmatic province. The Kangding Complex broadly overlaps other late Neoproterozoic magmatic rocks that are found throughout the west and northern borders of the Yangtze cratonic margin. There is limited $\varepsilon_{Hf}(t)$ data on other granitoids that intrude the

Table 1
LA-ICP-MS Lu-Hf isotope data (this study) with corresponding U-Pb spot ages (from Searle et al., 2016).

Sample	Spot	Age (Ma) $^{207}Pb/^{206}Pb$	2σ	Age (Ma) $^{206}Pb/^{238}U$	2σ	Total Hf (V)	$^{180}Hf/^{177}Hf$	2σ	$^{176}Yb/^{177}Hf$	2σ	$^{176}Lu/^{177}Hf$	2σ	$^{176}Hf/^{177}Hf$	2σ	$\varepsilon_{Hf}(t)$	2σ
BO52	B_01	132.4	36.5	15.2	0.5	10	1.886484	0.000146	0.026015	0.001795	0.000985	0.000108	0.282719	0.000036	−2.02	1.28
BO52	B_02	−18.9	26.8	41.9	0.9	32	1.886733	0.000078	0.029254	0.001202	0.000879	0.000018	0.282805	0.000031	1.60	1.08
BO52	B_03	34.7	24.8	40.5	1.1	19	1.886692	0.000090	0.021563	0.001452	0.000627	0.000008	0.282706	0.000032	−1.92	1.12
BO52	B_06	53.5	21.8	19.5	0.4	15	1.886763	0.000173	0.030188	0.003833	0.000816	0.000100	0.282667	0.000053	−3.76	1.87
BO52	B_08	156.9	44.5	160.2	4.4	14	1.886858	0.000123	0.021961	0.001273	0.000536	0.000045	0.282666	0.000033	−0.71	1.16
BO52	B_09	158.7	17.5	158.9	2.8	21	1.886717	0.000079	0.031845	0.001308	0.000833	0.000003	0.282631	0.000032	−2.01	1.14
BO52	B_10	57.0	24.9	17.5	0.4	13	1.886629	0.000166	0.036159	0.001287	0.000982	0.000070	0.282661	0.000048	−4.02	1.69
BO52	B_11	−16.8	31.3	17.6	0.4	18	1.886864	0.000102	0.023210	0.000821	0.000626	0.000021	0.282658	0.000031	−4.12	1.10
BO52	B_13	218.9	28.4	41.1	1.1	22	1.886846	0.000099	0.020255	0.001340	0.000608	0.000061	0.282743	0.000034	−0.60	1.20
BO62	B_01	638.1	44.6	64.5	3.2	22	1.886745	0.000087	0.012771	0.000327	0.000353	0.000006	0.282704	0.000031	−1.46	1.08
BO62	B_02	776.4	21.4	824.9	19.6	19	1.886803	0.000074	0.042714	0.001443	0.001095	0.000015	0.282565	0.000033	10.10	1.16
BO62	B_03	796.1	185.3	5.2	0.4	20	1.886774	0.000086	0.012101	0.000597	0.000330	0.000013	0.282838	0.000032	1.98	1.12
BO62	B_04	794.9	24.7	315.4	14.9	21	1.886731	0.000073	0.058623	0.001098	0.001693	0.000022	0.282533	0.000029	−2.25	1.03
BO62	B_08	275.4	99.1	5.4	0.3	21	1.886798	0.000097	0.015125	0.002364	0.000395	0.000052	0.282842	0.000029	2.12	1.03
BO62	B_09	161.7	81.1	5.3	0.2	25	1.886710	0.000086	0.020302	0.001316	0.000516	0.000033	0.282865	0.000032	2.93	1.12
BO62	B_15	−0.7	35.4	12.3	0.3	25	1.886850	0.000059	0.076630	0.002812	0.002317	0.000051	0.282831	0.000028	1.87	1.00
BO62	B_16	280.3	92.9	5.4	0.2	24	1.886802	0.000086	0.019170	0.000782	0.000498	0.000011	0.282789	0.000031	0.25	1.10
BO62	B_17	774.1	19.7	775.6	18.7	15	1.886776	0.000108	0.067250	0.001625	0.001871	0.000013	0.282555	0.000030	8.26	1.04
BO62	B_19	767.9	26.3	753.6	18.3	15	1.886798	0.000093	0.022109	0.001099	0.000649	0.000020	0.282515	0.000033	6.99	1.16
BO62	B_21	832.7	19.1	326.0	22.8	22	1.886860	0.000091	0.100611	0.001038	0.002733	0.000029	0.282556	0.000033	−1.44	1.18
BO62	B_22	850.3	22.1	794.5	17.6	15	1.886864	0.000082	0.037501	0.000279	0.000974	0.000008	0.282483	0.000032	6.59	1.12
BO62	B_25	507.3	110.7	5.8	0.3	25	1.886805	0.000071	0.013853	0.000404	0.000339	0.000003	0.282834	0.000030	1.85	1.06
BO62	C_01	748.4	24.1	713.8	16.8	21	1.886797	0.000099	0.028087	0.000717	0.000786	0.000028	0.282490	0.000029	5.16	1.01
BO62	C_02	740.4	23.9	780.8	19.5	18	1.886902	0.000073	0.045035	0.001092	0.001289	0.000015	0.282565	0.000030	9.03	1.04
BO62	C_04	716.7	98.3	541.9	28.6	17	1.886822	0.000094	0.009775	0.000560	0.000312	0.000011	0.282564	0.000031	4.17	1.08
BO62	C_11	364.4	173.3	5.9	0.4	18	1.886761	0.000100	0.020532	0.000838	0.000531	0.000018	0.282837	0.000031	1.96	1.08
BO62	C_12	799.4	20.7	783.3	16.1	16	1.886841	0.000085	0.086422	0.002572	0.002268	0.000009	0.282531	0.000030	7.37	1.04
BO62	C_14	799.4	19.6	769.7	13.5	18	1.886806	0.000072	0.093375	0.000976	0.002397	0.000035	0.282508	0.000032	6.20	1.14
BO62	C_15	797.9	23.2	760.5	17.6	18	1.886818	0.000101	0.045545	0.001967	0.001298	0.000028	0.282536	0.000030	7.56	1.04
BO62	C_17	780.1	25.1	778.3	18.7	19	1.886800	0.000126	0.082538	0.004518	0.002028	0.000054	0.282475	0.000031	5.40	1.10
BO62	C_19	1848.5	122.4	6.0	0.4	20	1.886766	0.000089	0.022793	0.001140	0.000581	0.000038	0.282728	0.000035	−1.90	1.23
BO62	C_21	766.7	28.3	370.7	11.9	28	1.886721	0.000074	0.023687	0.000162	0.000672	0.000016	0.282687	0.000029	4.63	1.01
BO62	C_36	814.6	20.1	750.3	15.4	20	1.886794	0.000081	0.045174	0.000227	0.001320	0.000023	0.282532	0.000031	7.18	1.08
BO62	C_39	827.1	123.1	7.0	0.5	22	1.886839	0.000072	0.017367	0.000245	0.000494	0.000004	0.282884	0.000034	3.64	1.20
BO62	C_40	744.7	34.5	685.3	15.5	16	1.886799	0.000076	0.022307	0.000780	0.000751	0.000020	0.282660	0.000032	10.57	1.14

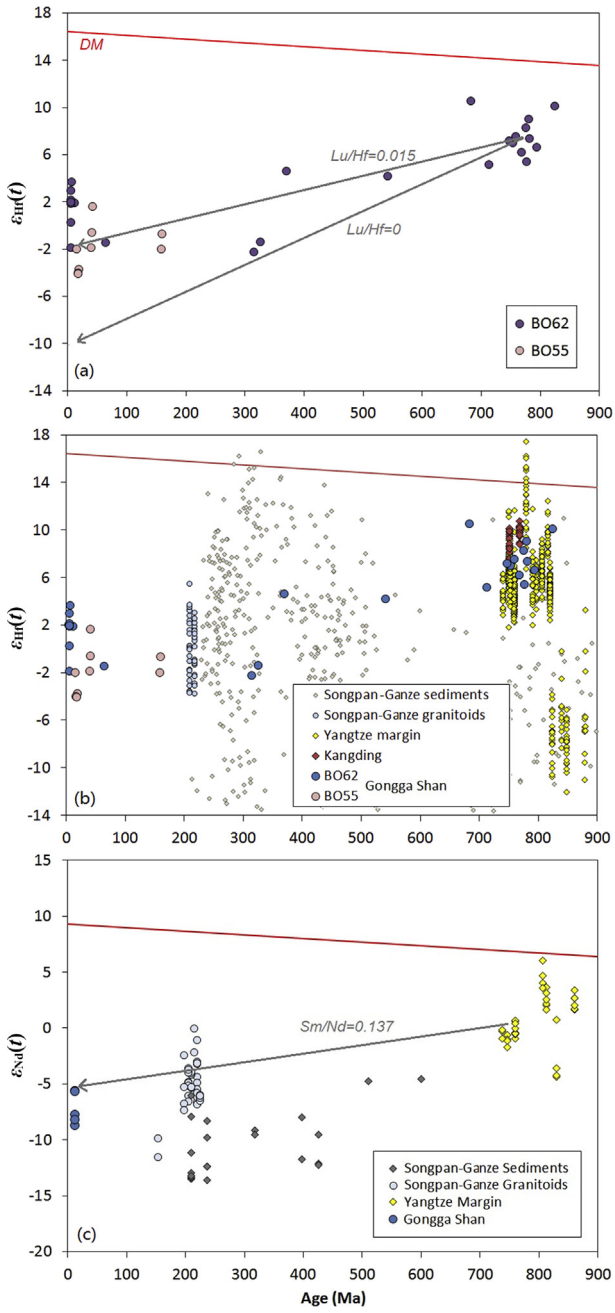

Figure 3. (a) $\varepsilon_{Hf}(t)$ vs. zircon age ($^{206}Pb/^{238}U$; Ma) for individual spot analyses (this study). (b) $\varepsilon_{Hf}(t)$ data for this study compared to potential source regions—Songpan–Ganze sediments (Zhang et al., 2014, 2015), Songpan–Ganze granitoids (Cai et al., 2009, 2010), Yangtze margin (Zheng et al., 2007; Zhao et al., 2008a; b; Wang et al., 2012), Kangding (Zheng et al., 2007). (c) $\varepsilon_{Nd}(t)$ vs. age for the Gongga Shan granitoids (Roger et al., 1995) compared to potential source regions Songpan–Ganze sediments (Chen et al., 2007; de Sigoyer et al., 2014), Songpan–Ganze granitoids (Roger et al., 2004; Xiao et al., 2007; Zhang et al., 2007; Cai et al., 2009, 2010; Yuan et al., 2010; de Sigoyer et al., 2014), Yangtze margin (Zhou et al., 2002; Zhao and Zhou, 2007a, b; Chen et al., 2015). DM = depleted mantle.

Songpan–Ganze terrane; the two Triassic analyses from Gongga Shan overlap these, implying a possible similarity in magmatic source, but there is also considerable spread in the other granitoids. The Triassic sedimentary rocks that form the cover of the Songpan–Ganze terrane have a wide range in $\varepsilon_{Hf}(t)$ values, and a broad range of Palaeozoic to Mesozoic ages. If these sedimentary signatures were averaged together, then their isotopic signature would overlap that of the Triassic and Oligocene–Miocene zircon domains in the Gongga Shan rocks. Whether this is likely will be discussed in the next section.

The $\varepsilon_{Nd}(t)$ signature of the rock suites shown in Fig. 3a–c. The plot shows that the SGT granitoids are compatible with reworking of a Neoproterozoic source region, as seen in the Hf plot, and the same applies to the Gongga Shan data. It should be noted that these latter data are not all directly dated, and plotted at the 12 Ma intrusion age that is reported by Roger et al. (1995). Interestingly, the SGT sediments have a much more limited range in $\varepsilon_{Nd}(t)$ space than $\varepsilon_{Hf}(t)$, and are distinctly more evolved than both the SGT granitoids and the Gongga Shan rocks.

6.2. Melting of neoproterozoic basement

The distinct $\varepsilon_{Nd}(t)$ and $\varepsilon_{Hf}(t)$ signature of the Miocene Gongga Shan magmatic rocks indicates that the Triassic SGT sediments that they intrude are not the most likely source, this in fact corresponds to a Neoproterozoic source, represented by the nearby Kangding Complex. Zircon inheritance data can be used to investigate this more thoroughly. A plot showing both all published magmatic crystallisation ages and all published in-situ zircon spot ages from Gongga Shan is shown in Fig. 4. It is clear that there is very little inheritance of Palaeozoic to Triassic ages that are dominant in the SGT flysch-type sediments (Weislogel et al., 2006, 2010; Zhang et al., 2014, 2015). Searle et al. (2016) inferred that the Gongga Shan intrusions were sourced from melting of this Triassic sedimentary fill, this is because these rocks would have been fertile (i.e. mica-rich) allowing for partial melt formation at moderate temperatures. Production of granitoids from melting of the Triassic SGT is one of the models inferred for granitoids found elsewhere across the SGT (Roger et al., 2004, 2010). This particularly accounts for the S-type nature of many of the granites, although it does not clearly explain the existence of several A- and I-types (Roger et al., 2004; Zhang et al., 2006, 2007; Xiao et al., 2007; Weislogel, 2008; Searle et al., 2016).

If we accept a Neoproterozoic source for the Gongga Shan granites as the data imply, then firstly we can infer that Neoproterozoic (Yangtze margin) crust underlies the region of the Gongga Shan batholith. The basement to the SGT has been debated (Roger et al., 2010 and references within), but is inferred by Roger

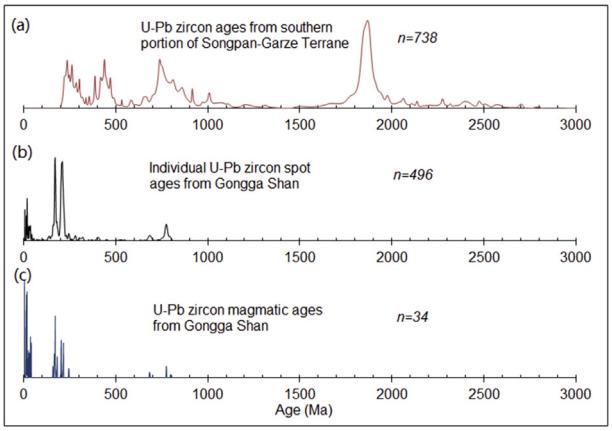

Figure 4. (a) Probability density plot of U–Pb detrital zircon ages from the southern portion of the Songpan–Ganze terrane (Weislogel et al., 2006, 2010; Zhang et al., 2014). (b) Probability density plot of U–Pb zircon spot ages for concordant (<10%) spot analyses from Gongga Shan (Li and Zhang, 2013; Li et al., 2015; Searle et al., 2016; Zhang et al., 2017). (c) Probability density plot of all U–Pb zircon magmatic ages from Gongga Shan (Roger et al., 1995; Liu et al., 2006; Li and Zhang, 2013; Li et al., 2015; Searle et al., 2016; Zhang et al., 2017).

et al. (2010) to be Neoproterozoic crust similar to the Yangtze craton, on the eastern edge of the SGT (Zhou et al., 2002). Gongga Shan, also located on the eastern border of the SGT, supports this model at least for the southern part of the SGT. The reason for melting of this Neoproterozoic crust remains enigmatic however. The Triassic–Jurassic intrusions may be related to: (1) crustal thickening and burial during the Indosinian orogeny (Roger et al., 2004, 2010); (2) a slab tear from opposing subduction zones either side of the SGT (de Sigoyer et al., 2014); (3) post-collisional delamination (Zhang et al., 2007); or (4) tearing of the thickened lower crust after infilling of the sedimentary basin (Yuan et al., 2010). The Oligocene–Miocene melts imply that over 100 Myrs later, during the on-going Himalaya–Tibetan orogeny, that the magmatic source region was reactivated or that new (but isotopically similar) source regions were partially melted; both possibilities may have involved decompression melting as a potential mechanism.

There is no clear surface geological evidence for Cenozoic metamorphism in the Gongga Shan region, or in fact the SGT as a whole. The deformation observed in the SGT sedimentary cover is inferred to be largely Indosinian (Harrowfield and Wilson, 2005). Weller et al. (2013) dated Barrovian burial metamorphism in the Danba region to the NE of Gongga Shan at 192 Ma (Staurolite-grade) to 174 Ma (Sillimanite-grade). Their study constrained what was previously thought to be a mixture of tectonothermal events based on scattered metamorphic ages (Huang et al., 2003a, b; Hou et al., 2012). Airaghi et al. (2017) identified an Early Jurassic greenschist metamorphism in the Pengguan massif along the Beichuan fault (Longmen Shan Fault Zone) at 140–135 Ma, which they argue is the onset of thick-skinned deformation in that region. Young movement within the Longmen Shan Fault Zone is known from the $M = 8$ 2008 Wenchuan earthquake and other smaller more recent movements (Hubbard and Shaw, 2009; Wang et al., 2014). Active deformation here is localised as steep faults that form a thick-skinned fold and thrust belt bounding the Sichuan Basin to the east (Hubbard et al., 2010; Li et al., 2010, 2014). This lack of widespread Cenozoic deformation and metamorphism in the SGT is in contrast to the south Tibetan margin, where the High Himalaya expose high-grade metamorphic rocks exhumed from the mid-crust, that are associated with large volumes of partial melt (see Searle et al., 2010; Cottle et al., 2015).

6.3. Comparison to other young melts

Gongga Shan does not represent the only young crustal melt in the Asian plate rocks of the Tibetan Plateau that is now exposed at the surface. Shown on Fig. 1b are three other known localities. The Western Nyainqentanglha mountains in the Lhasa terrane of Southern Tibet reveals distinct similarities to the Gongga Shan massif. Nyainqentanglha comprises sediments metamorphosed in the Triassic, which have been intruded by granitoids over a protracted history, ranging in age from ca. 213 Ma to 8 Ma (Xu et al., 1985; Liu et al., 2004; Kapp et al., 2005; Weller et al., 2016). The magmatic rocks were exhumed from the mid-crust (ca. 15–20 km in depth) since the late Neogene (Armijo et al., 1986; Harrison et al., 1995). The Lunggar Rift in south-west Tibet features granitoids formed between ca. 22 Ma and 8 Ma (Kapp et al., 2008). In Ulugh Muztagh, north Tibet, leucogranites formed at shallow levels (ca. 10 km) between ca. 10 Ma and 8 Ma, and intrude into Triassic sandstone (Burchfiel et al., 1989).

These crustal melt leucogranites located sporadically across the Asian plate side of the suture zone in Tibet are not the same as the Indian plate leucogranites, exposed along the Greater Himalaya (Searle et al., 2010) or the Yarlung suture zone (Laskowski et al., 2017). The Greater Himalayan Sequence (GHS) leucogranites are sourced and intruded into Indian plate rocks south of the suture zone. They are in situ melts from kyanite or silimanite ± cordierite migmatites and intruded as a vast network of sills and dykes in the GHS. The Tibetan leucogranites (although of similar age as the younger GHS melts) are different; they are melts derived from and intruded into rocks of the over-riding Asian plate, their source is deeper and generally not exposed, their geochemistry and isotopes distinctly different from the GHS, and they intrude older rocks of, for example, the Lhasa block. The Gongga Shan leucogranites are located much further north across at least another plate boundary (Bangong suture zone) and possibly yet another (Jinsha suture), and separated by hundreds of km where they are no known exposed Cenozoic leucogranites.

Weller et al. (2016) suggested that Nyainqentanglha, and by inference the other regions of young exposed crustal melting, may be exhumed examples of localised mid-crustal partial melts that can be seen in the middle crust of Tibet today as seismic-magnetotelluric 'bright spots'. These bright spots, recorded by INDEPTH seismic data (e.g. Brown et al., 1996; Makovsky et al., 1996; Wei et al., 2001), represent either melt or fluid (Makovsky and Klemperer, 1999; Unsworth et al., 2005), but either way, imply the existence of pockets of melt in the middle crust (Gaillard et al., 2004). Weller et al. (2016) suggested that their localisation is directly related to the existence of melt-fertile source rocks. This is intriguing given the case of Gongga Shan, where Neoproterozoic crust is inferred to be the magmatic source according to the present study. The melts forming the Gongga Shan leucogranites suggest that this Neoproterozoic 'basement' must comprise melt-fertile metasedimentary or meta-igneous units. The fact that young melts such as the Gongga Shan leucogranites are rarely seen in Asian plate rocks across the Tibetan plateau, is either due to the lack of melt-fertile rocks within the mid-crust, and/or to the lack of mechanisms to exhume and expose the crustal melts after they have formed. It may be that melt-fertile rocks produce melt during earlier stages of collisional orogeny, and that fertile regions remain scarce by late stages of orogeny. Both the Lunggar Rift and Nyainqentanglha, which is associated with the Yadong-Gulu Rift, are characterised by upper crustal extensional faulting, and hence, this could provide a mechanism to exhume the exposed melts (Kapp et al., 2008; Weller et al., 2016). However, the distribution of leucogranites away from the shallow normal faults that appear to cut them, suggests no direct link between Cenozoic upper crustal extension and crustal melting (Searle et al., 2011).

6.4. Exhuming Gongga Shan

Whereas the Lunggar Rift and Nyainqentanglha granitoids are associated with extensional rifts, the Gongga Shan batholith appears to be associated with the Xianshuihe strike-slip fault. This regional scale fault system, which features a series of onlapping strands as it transects the Gongga Shan batholith (see Fig. 1), cuts across all intrusions (Searle et al., 2016). Li and Zhang (2013) related Oligocene migmatisation in Gongga Shan to an earlier phase of movement, but it is not clear how the observed ductile fabric is related to the cross-cutting brittle fabric. Roger et al. (1995) inferred that the 12.8 Ma age they obtained for a Gongga Shan granite provided the age of onset of movement for the Xianshuihe fault. Searle et al. (2016) lowered this age to ca. 5 Ma, based on their youngest magmatic age. Recently, Zhang et al. (2017) provided another very young age from a similar part of the batholith at ca. 4 Ma, providing further confirmation of Pliocene magmatism.

The uplift history of Gongga Shan has been estimated by a range of techniques, comprising Rb–Sr, Ar–Ar and zircon and apatite fission tracks ages, most recently synthesised in Zhang et al. (2017). In their combined zircon and apatite fission track-based study,

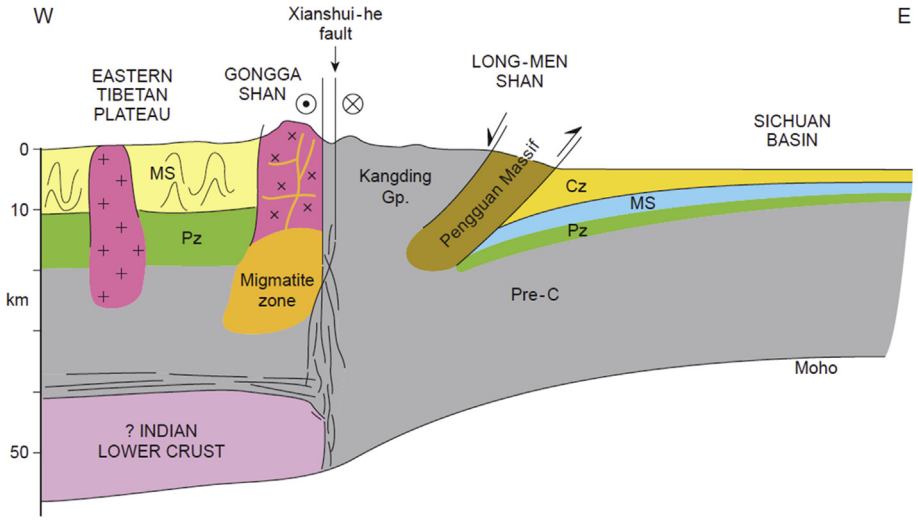

Figure 5. Sketch cross-section of a composite eastern Tibet–Gongga Shan–Sichuan basin profile showing crustal structure. In our speculative model, the lowermost crust is composed of underthrust Indian lower crust (Archaean granite). Triassic granites intrude the Palaeozoic–early Mesozoic sedimentary cover of eastern Tibet. Precambrian rocks crop out in eastern Tibet (Pengguan massif). The source for crustal melting in Gongga Shan is the Proterozoic mid-crust of Tibet. The eastern margin of the plateau is marked by the Long-Men Shan range, and steep-west-dipping thrust faults overthrusting the western margin of the Sichuan basin. CZ = Cenozoic; MS = Mesozoic; PZ = Palaeozoic; Pre-C = Precambrian.

Zhang et al. (2017) interpreted their data as recording rapid uplift commencing at 9 Ma, and slowing down since 4 Ma. Regionally, thermochronology has shown that the southeast Tibetan plateau (exclusive of the Namche Barwa syntaxis) has experienced little rock uplift and erosion since the Cretaceous (Lai et al., 2007; Zhang et al., 2017). The thermochronological data are interesting considering the geochronological ages of magmatism. They suggest that melting, presumably of the middle crust given the inferred Neoprotorozoic source, occurred both shortly before, and after, rapid exhumation of the massif. Zhang et al. (2017) also suggested that movement of the northern Yalahe strand of the Xianshuihe fault zone was active between 9 Ma and 4 Ma, i.e. before the youngest melts intruded.

In summary, we envisage the large-scale crustal structure in Fig. 5. Both Triassic and younger Gongga Shan components are presumed to be derived from Neoproterozoic source rocks underlying the region. The Triassic magmatism broadly overlapped and followed regional Indosinian deformation of the Songpan–Ganze sediments (e.g. Harrowfield and Wilson, 2005; Roger et al., 2010). Precambrian rocks crop out at the surface in eastern Tibet (Kangding complex) above crust possibly as thick as 60–65 km (Nabelek et al., 2009). This great thickness of Precambrian is best explained by Argand-type underplating of lower Indian crust beneath the south and central part of Tibet (Searle et al., 2011). The young Cenozoic melts intruding the older components of the Gongga Shan batholith were all uplifted by transpressional deformation associated with left-lateral strike-slip shearing along the Xianshuihe fault. Zhang et al. (2017) proposed that rapid exhumation started in the north of the batholith at ~9 Ma and slowed down since ~4 Ma. Our data suggest that young leucogranites occur along the eastern side of the batholith adjacent to the fault which cuts them, and hence we infer that rapid exhumation occurred since 5–4 Ma, whilst the surrounding plateau maintained its already ~5 km high elevation. Many of the Pliocene granites in Gongga Shan have younger crystallisation ages than the low-temperature thermochronological ages in the surrounding parts of the plateau (Zhang et al., 2017).

Surface- and body-wave tomography indicate that all of southern Tibet is underlain by high-velocity Indian crust (Preistley et al., 2008). Thermal models, combined with experimentally-derived flow laws suggest that if the Indian lower crust is anhydrous, it will remain strong as it progressively underplates the southern part of Tibet during convergence. Based on earthquake observations and thermal models, Craig et al. (2012) proposed that the 600 °C isotherm (the highest temperature cut-off for earthquakes) could extend horizontally for 450–500 km beneath the Tibetan plateau. Gongga Shan is approximately 350 km NE of the Eastern Himalayan syntaxis of definite Indian crustal origin. Searle et al. (2016) postulated that underthrust lower Indian crust (dry Archaean granulites) could have extended as far northeast as the Xianshuihe fault under eastern Tibet, and that this underthrusting and overthickening of the crust could explain the localised young mid-crustal melting at Gongga Shan (Fig. 5). The melt source for the young Cenozoic Gongga Shan leucogranites would lie in the mid-crust, the Asian plate Proterozoic basement gneisses above the lowermost crust comprised of Indian Shield-derived granulites (Fig. 5).

7. Conclusions

The source of young (ca. 15–4 Ma) crustal melts exposed in the Gongga Shan batholith, along the eastern margin of the Tibetan plateau, is interpreted to be Neoproterozoic crust equivalent to the adjacent Kangding Complex. This crust underlies the thick Triassic Songpan–Ganze sedimentary package locally, and perhaps across the region. Young melts require melt-fertile rocks, which may be sparse at this late stage of the collisional orogeny. The melts may be exhumed equivalents to the seismic-magnetotelluric “bright spots” imaged under other parts of the Tibetan Plateau. The process of their formation in this part of eastern Tibet remains enigmatic, although decompression melting is a plausible mechanism. Data shows that uplift is coincident with the latest magmatism, and it is inferred that regional structures play a role in exhumation. Underthrusting of India, rather than lower crustal flow, is one mechanism to uplift the region at this stage of the ongoing Himalayan-Tibetan orogeny. The final stage of exhumation of the Gongga Shan batholith with its young leucogranites was likely a result of transpression along the curved restraining bend of the dextral Xianshuihe strike-slip fault.

Acknowledgements

We thank the Institute of Geology, China Earthquake Administration, Beijing for assistance in the field. NR publishes with permission of the Executive Director of the British Geological Survey, UK.

References

Airaghi, L., de Sigoyer, J., Lanari, P., Guillot, S., Vidal, O., Monié, P., Sautter, B., Tan, X., 2017. Total exhumation across the Beichuan fault in the Longmen Shan (eastern Tibetan plateau, China): constraints from petrology and thermobarometry. Journal of Asian Earth Sciences 140, 108–121.

Armijo, R., Tapponnier, P., Mercier, J.L., Han, T.L., 1986. Quaternary extension in southern Tibet: field observations and tectonic implications. Journal of Geophysical Research: Solid Earth 91, 13803–13872.

Beaumont, C., Jamieson, R.A., Nguyen, M.H., Lee, B., 2001. Himalayan tectonics explained by extrusion of a low-viscosity crustal channel coupled to focused surface denudation. Nature 414, 738–742.

Bouvier, A., Vervoort, J.D., Patchett, P.J., 2008. The Lu–Hf and Sm–Nd isotopic composition of CHUR: constraints from unequilibrated chondrites and implications for the bulk composition of terrestrial planets. Earth and Planetary Science Letters 273, 48–57.

Bruguier, O., Lancelot, J.R., Malavieille, J., 1997. U–Pb dating on single detrital zircon grains from the Triassic Songpan–Ganze flysch (Central China): provenance and tectonic correlations. Earth and Planetary Science Letters 152, 217–231.

Brown, L.D., Zhao, W., Nelson, K.D., Hauck, M., 1996. Bright spots, structure, and magmatism in southern Tibet from INDEPTH seismic reflection profiling. Science 274, 1688.

Burchfiel, B.C., Molnar, P., Ziyun, Z., K'uangyi, L., Shuji, W., Minmin, H., Sutter, J., 1989. Geology of the Ulugh Muztagh area, northern Tibet. Earth and Planetary Science Letters 94, 57–70.

Cai, H., Zhang, H., Xu, W., 2009. U-Pb zircon ages, geochemical and Sr-Nd-Hf isotopic compositions of granitoids in western Songpan-Ganze fold belt: petrogenesis and implication for tectonic evolution. Journal of Earth Science 20, 681–698.

Cai, H., Zhang, H., Xu, W., Shi, Z., Yuan, H., 2010. Petrogenesis of Indosinian volcanic rocks in Songpan-Ganze fold belt of the northeastern Tibetan Plateau: new evidence for lithospheric delamination. Science China Earth Sciences 53, 1316–1328.

Chen, L., Booker, J.R., Jones, A.G., Wu, N., 1996. Electrically conductive crust in Southern Tibet form INDEPTH magnetotelluric surveying. Science 274, 1694.

Chen, Q., Sun, M., Long, X., Yuan, C., 2015. Petrogenesis of neoproterozoic adakitic tonalites and high-K granites in the eastern Songpan-Ganze fold belt and implications for the tectonic evolution of the western Yangtze block. Precambrian Research 270, 181–203.

Chen, Y., Liu, F., Zhang, H., Nie, L., Jiang, L., 2007. Elemental and Sm-Nd isotopic geochemistry on detrital sedimentary rocks in the Ganzi-Songpan block and Longmen Mountains. Frontiers of Earth Science in China 1, 60–68.

Chen, Z., Liu, Y., Hodges, K.V., Burchfiel, B.C., Royden, L.H., Deng, C., 1990. The Kangmar Dome: a metamorphic core complex in southern Xizang (Tibet). Science 250, 1552–1557.

Chen, Y., Luo, Z., Zhao, J., Li, Z., Zhang, H., Song, B., 2005. Petrogenesis and dating of the kangding complex, Sichuan Province. Science in China: Series D-Earth Sciences 48 (5), 622–634.

Chen, S.H.E., Wilson, C.J., Worley, B.A., 1995. Tectonic transition from the Songpan-Garzê fold belt to the Sichuan basin, south-western China. Basin Research 7, 235–253.

Chung, S.L., Chu, M.F., Zhang, Y., Xie, Y., Lo, C.H., Lee, T.Y., Lan, C.Y., Li, X., Zhang, Q., Wang, Y., 2005. Tibetan tectonic evolution inferred from spatial and temporal variations in post-collisional magmatism. Earth Science Reviews 68, 173–196.

Cottle, J.M., Larson, K.P., Kellett, D.A., 2015. How does the mid-crust accommodate deformation in large, hot collisional orogens? A review of recent research in the Himalayan orogen. Journal of Structural Geology 78, 119–133.

Craig, T.J., Copley, A., Jackson, J., 2012. Thermal and tectonic consequences of India underthusting Tibet. Earth and Planetary Science Letters 353–354, 231–239.

de Sigoyer, J., Vanderhaeghe, O., Duchêne, S., Billerot, A., 2014. Generation and emplacement of Triassic granitoids within the Songpan Ganze accretionary-orogenic wedge in a context of slab retreat accommodated by tear faulting, Eastern Tibetan plateau, China. Journal of Asian Earth Sciences 88, 192–216.

Decelles, P.G., Kapp, P., Gehrels, G.E., Ding, L., 2014. Paleocene-Eocene foreland basin evolution in the Himalaya of southern Tibet and Nepal: implications for the age of initial India-Asia collision. Tectonics 33, 824–849.

Ding, L., Yang, D., Cai, F.L., Pullen, A., Kapp, P., Gehrels, G.E., Zhang, L.Y., Zhang, Q.H., Lai, Q.Z., Yue, Y.H., Shi, R.D., 2013. Provenance analysis of the mesozoic Hoh-Xil-Songpan-Ganzi turbidites in northern Tibet: implications for the tectonic evolution of the eastern Paleo-Tethys ocean. Tectonics 32, 34–48.

Enkelmann, E., Weislogel, A., Ratschbacher, L., Eide, E., Renno, A., Wooden, J., 2007. How was the Triassic Songpan-Ganzi basin filled? A provenance study. Tectonics 26.

Fisher, C.M., Hanchar, J.M., Samson, S.D., Dhuime, B., Blichert-Toft, J., Vervoort, J.D., Lam, R., 2011. Synthetic zircon doped with hafnium and rare earth elements: a reference material for in situ hafnium isotope analysis. Chemical Geology 286, 32–47.

Gaillard, F., Scaillet, B., Pichavant, M., 2004. Evidence for present-day leucogranite pluton growth in Tibet. Geology 32, 801–804.

Gehrels, G., Kapp, P., DeCelles, P., Pullen, A., Blakey, R., Weislogel, A., Ding, L., Guynn, J., Martin, A., McQuarrie, N., Yin, A., 2011. Detrital zircon geochronology of pre-Tertiary strata in the Tibetan-Himalayan orogen. Tectonics 30.

Green, O.R., Searle, M.P., Corfield, R.I., Corfield, R.M., 2008. Cretaceous-Tertiary carbonate platform evolution and the age of the India-Asia collision along the Ladakh Himalaya (Northwest India). The Journal of Geology 116, 331–353.

Griffin, W.L., Wang, X., Jackson, S.E., Pearson, N.J., O'Reilly, S.Y., Xu, X., Zhou, X., 2002. Zircon chemistry and magma mixing, SE China: in-situ analysis of Hf isotopes, Tonglu and Pingtan igneous complexes. Lithos 61, 237–269.

Grujic, D., Hollister, L.S., Parrish, R.R., 2002. Himalayan metamorphic sequence as an orogenic channel: insight from Bhutan. Earth and Planetary Science Letters 198, 177–191.

Guo, Z., Wilson, M., Liu, J., Mao, Q., 2006. Post-collisional, potassic and ultrapotassic magmatism of the northern Tibetan Plateau: constraints on characteristics of the mantle source, geodynamic setting and uplift mechanisms. Journal of Petrology 47, 1177–1220.

Harrison, T.M., Copeland, P., Kidd, W.S.F., Lovera, O.M., 1995. Activation of the Nyainqentanghla shear zone: implications for uplift of the southern Tibetan Plateau. Tectonics 14, 658–676.

Harrowfield, M.J., Wilson, C.J., 2005. Indosinian deformation of the Songpan Ganze fold belt, northeast Tibetan Plateau. Journal of Structural Geology 27, 101–117.

Hodges, K.V., 2000. Tectonics of the Himalaya and southern Tibet from two perspectives. Geological Society of America Bulletin 112, 324–350.

Hollister, L.S., Crawford, M.L., 1986. Melt-enhanced deformation: a major tectonic process. Geology 14, 558–561.

Hou, Z.Q., Zheng, Y.C., Zeng, L.S., Gao, L.E., Huang, K.X., Li, W., Li, Q.Y., Fu, Q., Liang, W., Sun, Q.Z., 2012. Eocene–Oligocene granitoids in southern Tibet: constraints on crustal anatexis and tectonic evolution of the Himalayan orogen. Earth and Planetary Science Letters 349, 38–52.

Hu, X., Garzanti, E., Wang, J., Huang, W., An, W., Webb, A., 2016. The timing of India-Asia collision onset–Facts, theories, controversies. Earth-Science Reviews 160, 264–299.

Huang, M.H., Buick, I.S., Hou, L.W., 2003a. Tectonometamorphic evolution of the eastern Tibet plateau: evidence from the central Songpan–Garzê orogenic belt, Western China. Journal of Petrology 44, 255–278.

Huang, M., Maas, R., Buick, I.S., Williams, I.S., 2003b. Crustal response to continental collisions between the Tibet, Indian, South China and North China blocks: geochronological constraints from the Songpan-Ganze orogenic belt, western China. Journal of Metamorphic Geology 21, 223–240.

Hubbard, J., Shaw, J.H., 2009. Uplift of the Longmen Shan and Tibetan plateau, and the 2008 Wenchuan (M= 7.9) earthquake. Nature 458, 194–197.

Hubbard, J., Shaw, J.H., Klinger, Y., 2010. Structural setting of the 2008 Mw 7.9 Wenchuan, China, earthquake. Bulletin of the Seismological Society of America 100 (5B), 2713–2735.

Jamieson, R.A., Unsworth, M.J., Harris, N.B., Rosenberg, C.L., Schulmann, K., 2011. Crustal melting and the flow of mountains. Elements 7 (4), 253–260.

Kapp, J.L.A., Harrison, T.M., Kapp, P., Grove, M., Lovera, O.M., Lin, D., 2005. Nyainqentanglha Shan: a window into the tectonic, thermal, and geochemical evolution of the Lhasa block, southern Tibet. Journal of Geophysical Research: Solid Earth 110 (B8).

Kapp, P., Taylor, M., Stockli, D., Ding, L., 2008. Development of active low-angle normal fault systems during orogenic collapse: insight from Tibet. Geology 36, 7–10.

King, J., Harris, N., Argles, T., Parrish, R., Zhang, H., 2011. Contribution of crustal anatexis to the tectonic evolution of Indian crust beneath southern Tibet. Geological Society of America Bulletin 123, 218–239.

Lai, Q., Ding, L., Wang, H., Yue, Y., Cai, F., 2007. Constraining the stepwise migration of the eastern Tibetan Plateau margin by apatite fission track thermochronology. Science in China: Series D-Earth Sciences 50, 172–183.

Laskowski, A.K., Kapp, P., Ding, L., Campbell, C., Liu, X., 2017. Tectonic evolution of the Yarlung suture zone, Lopu Range region, southern Tibet. Tectonics 36, 108. https://doi.org/10.1002/2016TC004334.

Li, H., Zhang, Y., 2013. Zircon U–Pb geochronology of the Konggar granitoid and migmatite: constraints on the Oligo-Miocene tectono-thermal evolution of the Xianshuihe fault zone, East Tibet. Tectonophysics 606, 127–139.

Li, H., Zhang, Y., Zhang, C., Dong, S., Zhu, F., 2015. Middle Jurassic syn-kinematic magmatism, anatexis and metamorphism in the Zheduo-Gonggar massif, implication for the deformation of the Xianshuihe fault zone, East Tibet. Journal of Asian Earth Sciences 107, 35–52.

Li, S., Unsworth, M.J., Booker, J.R., Wei, W., Tan, H., Jones, A.G., 2003. Partial melt or aqueous fluid in the mid-crust of Southern Tibet? Constraints from INDEPTH magnetotelluric data. Geophysical Journal International 153, 289–304.

Li, Y., Jia, D., Shaw, J.H., Hubbard, J., Lin, A., Wang, M., Luo, L., Li, H., Wu, L., 2010. Structural interpretation of the coseismic faults of the Wenchuan earthquake: three-dimensional modeling of the Longmen Shan fold-and-thrust belt. Journal of Geophysical Research: Solid Earth 115.

Li, Y., Jia, D., Wang, M., Shaw, J.H., He, J., Lin, A., Xiong, L., Rao, G., 2014. Structural geometry of the source region for the 2013 Mw 6.6 Lushan earthquake: implication for earthquake hazard assessment along the Longmen Shan. Earth and Planetary Science Letters 390, 275–286.

Liu, S.W., Wang, Z.Q., Yan, Q.R., Li, Q.G., Zhang, D.H., Wang, J.G., 2006. Timing, petrogenesis and geodynamic significance of Zheduoshan Granitoids. Acta Petrologica Sinica 22, 343–352.
Liu, Q., Wu, Z., Hu, D., Ye, P., Jiang, W., Wang, Y., Zhang, H., 2004. SHRIMP U-Pb zircon dating on Nyainqentanglha granite in central Lhasa block. Chinese Science Bulletin 49, 76–82.
Makovsky, Y., Klemperer, S.L., 1999. Measuring the seismic properties of Tibetan bright spots: evidence for free aqueous fluids in the Tibetan middle crust. Journal of Geophysical Research Solid Earth 104, 10795–10825.
Makovsky, Y., Klemperer, S.L., Ratschbacher, L., Brown, L.D., Li, M., Zhao, W., Meng, F., 1996. INDEPTH wide-angle reflection observation of P-wave-to-S-wave conversion from crustal bright spots in Tibet. Science 274, 1690–1692.
Miller, C., Schuster, R., Klötzli, U., Frank, W., Purtscheller, F., 1999. Post-collisional potassic and ultrapotassic magmatism in SW Tibet: geochemical and Sr–Nd–Pb–O isotopic constraints for mantle source characteristics and petrogenesis. Journal of Petrology 40, 1399–1424.
Nabelek, J., Hétenyi, G., Vergne, J., et al., 2009. Underplating in the Himalaya-Tibet collision zone revealed by the Hi-CLIMB experiment. Science 325, 1371–1374.
Najman, Y., Appel, E., Boudagher-Fadel, M., Bown, P., Carter, A., Garzanti, E., Godin, L., Han, J., Liebke, U., Oliver, G., Parrish, R., 2010. Timing of India-Asia collision: geological, biostratigraphic, and palaeomagnetic constraints. Journal of Geophysical Research: Solid Earth 115 (B12).
Najman, Y., Jenks, D., Godin, L., Boudagher-Fadel, M., Millar, I., Garzanti, E., Horstwood, M., Bracciali, L., 2017. The Tethyan Himalayan detrital record shows that India–Asia terminal collision occurred by 54 Ma in the Western Himalaya. Earth and Planetary Science Letters 459, 301–310.
Nelson, K.D., Zhao, W., Brown, L.D., Kuo, J., 1996. Partially molten middle crust beneath southern Tibet: synthesis of project INDEPTH results. Science 274, 1684.
Nowell, G., Parrish, R.R., 2001. Simultaneous acquisitionof isotope compositions and parent/daughter ratios by non-isotope dilution-modePlasma Ionisation Multi-collector Mass Spectrometry (PIMMS). Special Publication-Royal Society Of Chemistry 267 (1), 298–310.
Preistley, K., Jackson, J., McKenzie, D., 2008. Lithospheric structure and deep earthquakes beneath India, the Himalaya and southern Tibet. Geophysical Journal International 172, 345–362.
Roger, F., Calassou, S., Lancelot, J., Malavieille, J., Mattauer, M., Zhiqin, X., Ziwen, H., Liwei, H., 1995. Miocene emplacement and deformation of the Konga Shan granite (Xianshui He fault zone, west Sichuan, China): geodynamic implications. Earth and Planetary Science Letters 130, 201–216.
Roger, F., Jolivet, M., Malavieille, J., 2010. The tectonic evolution of the Songpan-Garzê (North Tibet) and adjacent areas from Proterozoic to Present: a synthesis. Journal of Asian Earth Sciences 39, 254–269.
Roger, F., Malavieille, J., Leloup, P.H., Calassou, S., Xu, Z., 2004. Timing of granite emplacement and cooling in the Songpan–Garzê Fold Belt (eastern Tibetan Plateau) with tectonic implications. Journal of Asian Earth Sciences 22, 465–481.
Rosenberg, C.L., Handy, M.R., 2005. Experimental deformation of partially melted granite revisited: implications for the continental crust. Journal of Metamorphic Geology 23, 19–28.
Searle, M.P., Cottle, J.M., Streule, M.J., Waters, D.J., 2010. Crustal melt granites and migmatites along the Himalaya: melt source, segregation, transport and granite emplacement mechanisms. Geological Society of America Special Papers 472, 219–233.
Searle, M.P., Elliott, J.R., Phillips, R.J., Chung, S.-L., 2011. Crustal – lithospheric structure and continental extrusion of Tibet. Journal of the Geological Society, London 168, 633–672. https://doi.org/10.1144/0016-76492010-139.
Searle, M.P., Law, R.D., Jessup, M.J., 2006. Crustal structure, restoration and evolution of the Greater Himalaya in Nepal-South Tibet: implications for channel flow and ductile extrusion of the middle crust. Geological Society, London, Special Publications 268, 355–378.
Searle, M.P., Roberts, N.M., Chung, S.L., Lee, Y.H., Cook, K.L., Elliott, J.R., Weller, O.M., St-Onge, M.R., Xu, X.W., Tan, X.B., Li, K., 2016. Age and anatomy of the Gongga Shan batholith, eastern Tibetan Plateau, and its relationship to the active Xianshui-he fault. Geosphere 12, 948–970.
Sláma, J., et al., 2008. Plešovice zircon—a new natural reference material for U–Pb and Hf isotopic microanalysis. Chemical Geology 249, 1–35.
Söderlund, U., Patchett, P.J., Vervoort, J.D., Isachsen, C.E., 2004. The 176 Lu decay constant determined by Lu–Hf and U–Pb isotope systematics of Precambrian mafic intrusions. Earth and Planetary Science Letters 219, 311–324.
Streule, M.J., Searle, M.P., Waters, D.J., Horstwood, M.S., 2010. Metamorphism, melting, and channel flow in the Greater Himalayan Sequence and Makalu leucogranite: constraints from thermobarometry, metamorphic modeling, and U-Pb geochronology. Tectonics 29, TC5011. https://doi.org/10.1029/2009TC002533.
Unsworth, M.J., Jones, A.G., Wei, W., Marquis, G., Gokarn, S.G., Spratt, J.E., Bedrosian, P., Booker, J., Leshou, C., Clarke, G., Shenghui, L., 2005. Crustal rheology of the Himalaya and Southern Tibet inferred from magnetotelluric data. Nature 438, 78–81.
Wang, Z., Huang, R., Pei, S., 2014. Crustal deformation along the Longmen-Shan fault zone and its implications for seismogenesis. Tectonophysics 610, 128–137.
Wang, W., Liu, S., Feng, Y., Li, Q., Wu, F., Wang, Z., Wang, R., Yang, P., 2012. Chronology, petrogenesis and tectonic setting of the Neoproterozoic Tongchang dioritic pluton at the northwestern margin of the Yangtze Block: constraints from geochemistry and zircon U–Pb–Hf isotopic systematics. Gondwana Research 22, 699–716.
Wei, W., Unsworth, M., Jones, A., Booker, J., Tan, H., Nelson, D., Chen, L., Li, S., Solon, K., Bedrosian, P., Jin, S., 2001. Detection of widespread fluids in the Tibetan crust by magnetotelluric studies. Science 292, 716–719.
Weislogel, A.L., 2008. Tectonostratigraphic and geochronologic constraints on evolution of the northeast Paleotethys from the Songpan-Ganzi complex, central China. Tectonophysics 451 (1), 331–345.
Weislogel, A.L., Graham, S.A., Chang, E.Z., Wooden, J.L., Gehrels, G.E., Yang, H., 2006. Detrital zircon provenance of the late Triassic Songpan-Ganzi complex: sedimentary record of collision of the north and south China blocks. Geology 34, 97–100.
Weislogel, A.L., Graham, S.A., Chang, E.Z., Wooden, J.L., Gehrels, G.E., 2010. Detrital zircon provenance from three turbidite depocenters of the Middle–Upper Triassic Songpan-Ganzi complex, central China: record of collisional tectonics, erosional exhumation, and sediment production. Geological Society of America Bulletin 122, 2041–2062.
Weller, O.M., St-Onge, M.R., Waters, D.J., Rayner, N., Searle, M.P., Chung, S.-L., Palin, R.M., Lee, Y.-H., Xu, X., 2013. Quantifying Barrovian metamorphism in the Danba structural culmination of eastern Tibet. Journal of Metamorphic Geology. https://doi.org/10.1111/jmg.12050.
Weller, O.M., St-Onge, M.R., Rayner, N., Searle, M.P., Waters, D.J., 2016. Miocene magmatism in the Western Nyainqentanglha mountains of southern Tibet: an exhumed bright spot? Lithos 245, 147–160.
Wiedenbeck, M.A.P.C., et al., 1995. Three natural zircon standards for U-Th-Pb, Lu-Hf, trace element and REE analyses. Geostandards Newsletter 19, 1–23.
Wiedenbeck, M.A.P.C., et al., 2004. Further characterisation of the 91500 zircon crystal. Geostandards and Geoanalytical Research 28, 9–39.
Williams, H.M., Turner, S.P., Pearce, J.A., Kelley, S.P., Harris, N.B.W., 2004. Nature of the source regions for post-collisional, potassic magmatism in southern and northern Tibet from geochemical variations and inverse trace element modelling. Journal of Petrology 45, 555–607.
Xiao, L., Zhang, H.F., Clemens, J.D., Wang, Q.W., Kan, Z.Z., Wang, K.M., Ni, P.Z., Liu, X.M., 2007. Late Triassic granitoids of the eastern margin of the Tibetan Plateau: geochronology, petrogenesis and implications for tectonic evolution. Lithos 96, 436–452.
Xu, R.H., Schärer, U., Allègre, C.J., 1985. Magmatism and metamorphism in the Lhasa block (Tibet): a geochronological study. The Journal of Geology 93, 41–57.
Yuan, C., Zhou, M.F., Sun, M., Zhao, Y., Wilde, S., Long, X., Yan, D., 2010. Triassic granitoids in the eastern Songpan Ganzi Fold Belt, SW China: magmatic response to geodynamics of the deep lithosphere. Earth and Planetary Science Letters 290, 481–492.
Zeng, L., Gao, L.E., Xie, K., Liu-Zeng, J., 2011. Mid-Eocene high Sr/Y granites in the Northern Himalayan Gneiss Domes: melting thickened lower continental crust. Earth and Planetary Science Letters 303, 251–266.
Zhang, H.F., Parrish, R., Zhang, L., Xu, W.C., Yuan, H.L., Gao, S., Crowley, Q.G., 2007. A-type granite and adakitic magmatism association in Songpan–Ganze fold belt, eastern Tibetan Plateau: implication for lithospheric delamination. Lithos 97, 323–335.
Zhang, H.F., Zhang, L., Harris, N., Jin, L.L., Yuan, H., 2006. U–Pb zircon ages, geochemical and isotopic compositions of granitoids in Songpan-Ganze fold belt, eastern Tibetan Plateau: constraints on petrogenesis and tectonic evolution of the basement. Contributions to Mineralogy and Petrology 152 (1), 75–88.
Zhang, Y.X., Tang, X.C., Zhang, K.J., Zeng, L., Gao, C.L., 2014. U–Pb and Lu–Hf isotope systematics of detrital zircons from the Songpan–Ganzi Triassic flysch, NE Tibetan Plateau: implications for provenance and crustal growth. International Geology Review 56, 29–56.
Zhang, Y.X., Zeng, L., Li, Z.W., Wang, C.S., Zhang, K.J., Yang, W.G., Guo, T.L., 2015. Late Permian–Triassic siliciclastic provenance, palaeogeography, and crustal growth of the Songpan terrane, eastern Tibetan Plateau: evidence from U–Pb ages, trace elements, and Hf isotopes of detrital zircons. International Geology Review 57, 159–181.
Zhang, Y.Z., Replumaz, A., Leloup, P.H., Wang, G.C., Bernet, M., van der Beek, P., Paquette, J.L., Chevalier, M.L., 2017. Cooling history of the Gongga batholith: implications for the Xianshuihe fault and Miocene kinematics of SE Tibet. Earth and Planetary Science Letters 465, 1–15.
Zhao, J.H., Zhou, M.F., 2007a. Geochemistry of Neoproterozoic mafic intrusions in the Panzhihua district (Sichuan Province, SW China): implications for subduction-related metasomatism in the upper mantle. Precambrian Research 152, 27–47.
Zhao, J.H., Zhou, M.F., 2007b. Neoproterozoic adakitic plutons and arc magmatism along the western margin of the Yangtze Block, South China. The Journal of Geology 115, 675–689.
Zhao, J.H., Zhou, M.F., Yan, D.P., Yang, Y.H., Sun, M., 2008a. Zircon Lu–Hf isotopic constraints on Neoproterozoic subduction-related crustal growth along the western margin of the Yangtze Block, South China. Precambrian Research 163, 189–209.
Zhao, X.F., Zhou, M.F., Li, J.W., Wu, F.Y., 2008b. Association of Neoproterozoic A-and I-type granites in South China: implications for generation of A-type granites in a subduction-related environment. Chemical Geology 257 (1), 1–15.
Zheng, Y.F., Zhang, S.B., Zhao, Z.F., Wu, Y.B., Li, X., Li, Z., Wu, F.Y., 2007. Contrasting zircon Hf and O isotopes in the two episodes of Neoproterozoic granitoids in South China: implications for growth and reworking of continental crust. Lithos 96, 127–150.
Zhou, M.F., Yan, D.P., Kennedy, A.K., Li, Y., Ding, J., 2002. SHRIMP U–Pb zircon geochronological and geochemical evidence for Neoproterozoic arc-magmatism along the western margin of the Yangtze Block, South China. Earth and Planetary Science Letters 196 (1), 51–67.